REPORT DOCUMENTATION PAGE

Form Approved
OMB NO. 0704-0188

1. AGENCY USE ONLY (Leave Blank)	2. REPORT DATE	3. REPORT TYPE AND DATES COVERED
		Peer Reviewed Reprint

4. TITLE AND SUBTITLE
Errors in Numerical Solutions of Spherically Symmetric Shock Physics Problems

5. FUNDING NUMBERS
DAAD19-01-1-0642

6. AUTHOR(S) James Glimm, John W. Grove, Yunghee Kang, Taewon Lee, Xiaolin Li, David H. Sharp, Kenny Q. Ye, Yan Yu, and Ming Zhao

7. PERFORMING ORGANIZATION NAME(S) AND ADDRESS(ES)
Research Foundation of SUNY at Stony Brook
Department of Applied Math. & Statistics
Stony Brook, NY 11794-3600

8. PERFORMING ORGANIZATION REPORT NUMBER

9. SPONSORING / MONITORING AGENCY NAME(S) AND ADDRESS(ES)
U. S. Army Research Office
P.O. Box 12211
Research Triangle Park, NC 27709-2211

10. SPONSORING / MONITORING AGENCY REPORT NUMBER
42254.40-MA

11. SUPPLEMENTARY NOTES
The views, opinions and/or findings contained in this report are those of the author(s) and should not be construed as an official Department of the Army position, policy or decision, unless so designated by other documentation.

12 a. DISTRIBUTION / AVAILABILITY STATEMENT
Approved for public release; distribution unlimited.

12 b. DISTRIBUTION CODE

13. ABSTRACT (Maximum 200 words) We seek robust and understandable error models for shock physics simulations. The purpose of this paper is to explore complications introduced by spherical flow in the analysis of errors in the numerical solution of shock interaction problems. In contrast to the case of planar waves, the spherical waves are not constant in strength between interactions and the solution is not piecewise constant between waves. Nevertheless simple power laws predict the dependence of the solution on the radius. We find that the same power laws predict the evolution of the error, as the error, once formed, propagates according to the same laws as govern the solution structures (i.e. the waves) themselves. We analyze errors in composite wave interaction problems based on the analysis of single interactions and a multi-path scattering formula to combine the effects of errors propagating through the individual interactions.

We refine the wave filters we have previously introduced for the identification

14. SUBJECT TERMS	15. NUMBER OF PAGES	16. PRICE CODE
	17	

17. SECURITY CLASSIFICATION OR REPORT	18. SECURITY CLASSIFICATION ON THIS PAGE	19. SECURITY CLASSIFICATION OF ABSTRACT	20. LIMITATION OF ABSTRACT
UNCLASSIFIED	UNCLASSIFIED	UNCLASSIFIED	UL

NSN 7540-01-280-5500

Standard Form 298 (Rev.2-89)
Prescribed by ANSI Std. 239-18
298-102

Enclosure 1

REPORT DOCUMENTATION PAGE (SF298)
(Continuation Sheet)

RE: Errors in Numerical Solutions of Spherically Symmetric Shock Physics Problems

and analysis of wave strength and position in planar (1D) shock physics simulations. The filter now must be applicable to the case of non-constant states between waves. The numerical solutions in contrast to the physical solutions, are approximately constant in a narrow region immediately adjacent to the numerical waves. For this reason, the planar one dimensional wave filters provide sufficient accuracy and are used without change. However, as we contemplate the solution of the same problem in a two dimensional cylindrical geometry (r,z) or three dimensional rectangular geometry (x, y, z) and also the solutions of perturbed spherical problems, such as the spherical Richtmyer-Meshkov instability problem, there will be a need for higher dimensional wave filters. We offer a solution to this pattern recognition problem.

Contemporary Mathematics

Errors in Numerical Solutions of Spherically Symmetric Shock Physics Problems

James Glimm, John W. Grove, Yunghee Kang, Taewon Lee, Xiaolin Li, David H. Sharp, Kenny Q. Ye, Yan Yu, and Ming Zhao

ABSTRACT. We seek robust and understandable error models for shock physics simulations. The purpose of this paper is to explore complications introduced by spherical flow in the analysis of errors in the numerical solution of shock interaction problems. In contrast to the case of planar waves, the spherical waves are not constant in strength between interactions and the solution is not piecewise constant between waves. Nevertheless simple power laws predict the dependence of the solution on the radius. We find that the same power laws predict the evolution of the error, as the error, once formed, propagates according to the same laws as govern the solution structures (*i.e.* the waves) themselves. We analyze errors in composite wave interaction problems based on the analysis of single interactions and a multi-path scattering formula to combine the effects of errors propagating through the individual interactions.

We refine the wave filters we have previously introduced for the identification and analysis of wave strength and position in planar (1D) shock physics simulations. The filter now must be applicable to the case of non-constant states between waves. The numerical solutions, in contrast to the physical solutions, are approximately constant in a narrow region immediately adjacent to the numerical waves. For this reason, the planar one dimensional wave filters provide sufficient accuracy and are used without change. However, as we contemplate the solution of the same problem in a two dimensional cylindrical geometry (r, z) or three dimensional rectangular geometry (x, y, z) and also the solutions of perturbed spherical problems, such as the spherical Richtmyer-Meshkov instability problem, there will be a need for higher dimensional wave filters. We offer a solution to this pattern recognition problem.

1991 *Mathematics Subject Classification.* Primary 65Z05; Secondary 65G99, 76L05.

Key words and phrases. Uncertainty quantification, spherical shock wave interactions, composition law, Guderley solution.

J. Glimm was supported in part by the NSF Grant DMS-0102480 and the U. S. Department of Energy Grant DE-AC02-98CH10886.

J. Glimm, T. Lee, Y. Yu and M. Zhao were supported in part by the Army Research Office Grant DAAD-190110642, the U.S. Department of Energy Grant DE-FG02-90ER25084 and the U.S. Department of Energy Grant DE-FG03-98DP00206.

J. W. Grove, Y. Kang and D. H. Sharp were supported by the U.S. Department of Energy.

X. Li was supported in part by U.S. Department of Energy Grant DEFC02-01ER25461.

1. Introduction

We are concerned with the identification and characterization of solution errors in spherically symmetric shock interaction problems. This issue applies to the study of supernova and the design of inertial confinement fusion (ICF) capsules. In the first case, theory and simulations contain a number of uncertainties, and comparison to observations is thus not definitive. A systematic effort to remove some of the uncertainties associated with simulation will thus be a useful contribution. In the second case of ICF design, concern over solution accuracy has led to mandates of formal efforts to assure solution accuracy.

In previous papers, we have developed a general approach to uncertainty and numerical solution error [**5, 6**], and we have analyzed shock interactions in a planar geometry [**2, 4**]. Here we focus specifically on complications which result from spherical geometry. In brief, these are:

(1) The solution waves are not of constant strength between wave interactions, but evolve approximately according to a power law as a function of the radius.
(2) The solution is not spatially constant between waves.
(3) If the solution is not required to be spherically symmetric, the problem of identifying wave structures as curves or surfaces in 2D or 3D is introduced.

These are classical problems as far as the solutions are concerned, but the application of these ideas to the analysis of errors in the solution appears to be new. The radially dependent strength of spherical waves is discussed in [**8**]. The spatial variation of spherical waves is contained in the Guderley solution [**7**].

The problem of analysis of errors in numerical solutions is of course central to numerical analysis. Much of this effort is motivated by other concerns, and appears not to be directly applicable to the problems we address.

An early focus of numerical error modeling was round off errors. For the hyperbolic systems we study, modern 64-bit processors with double precision arithmetic appear, as a practical matter, not to be sensitive to this class of errors, while they are difficult to analyze theoretically. A more common approach to error analysis in numerical analysis is the study of the asymptotic behavior of errors under mesh refinement. This is a useful approach, and one we refer to in the case of well resolved simulations. However, we want an analysis which is also applicable to the pre-asymptotic case of under resolved simulations as these are so typical of practical studies of realistic complex physical systems. Moreover, the coefficients which multiply powers of Δx in the asymptotic expressions cannot be determined theoretically. A third main theme in the analysis of errors is the use of *a posteriori* error estimators. These are upper bounds on the error in the solution, based on criteria derived from the (approximate) solution and the exact equation only. Such a study comes close to the problems we address, but differs in a few respects. We seek to characterize the error, not just to bound it. Moreover, *a posteriori* methods are most fully developed and justified theoretically for elliptic problems, and have only a partial or preliminary development for the shock interaction problems we consider here. A fourth approach to errors is to regard them as due to input uncertainties. In this point of view, uncertainty analysis is a mapping of input random variables to output random variables.

In contrast to the first three of the above methods, we analyze the errors statistically. The statistical models are simple, and in this sense, we analyze only the central portion of the error statistics, not their tails. We use a Gaussian error model, and thus we identify the mean error and the covariance. The mean error is a systematic error, and it can in principle be used to modify or "post process" and error-correct the approximate solution. The covariance is a measure of the error variability. One may question the idea that numerical errors can be modeled statistically or that the errors are variable, when each simulation is totally deterministic. This philosophical question has an easy answer: determinism lies in the eye of the beholder. In other words, the modeling of a natural phenomena (tossing a coin, for example) as a probabilistic or deterministic event depends on the level of detail included or excluded from the model. Thus we argue only why it is convenient or nearly essential to omit from the modeling of error information needed to make the error analysis deterministic. The variable (as opposed to the systematic) part of the error depends on "accidental" features of the numerical model, such as the sub grid location of waves and wave interaction points relative to the mesh cell edges. Clearly a deterministic model requiring such data would be too cumbersome for use in practice, and thus a probabilistic model is preferable. Indeed, the essentially probabilistic aspect of round off error is well recognized. Given that the complexity of a statistical model is needed, we found that simple linear error models were sufficient for our analysis [4]. The simple reason for this pleasant turn of events is that the error is similar to a perturbation, and normally a small perturbation. Thus the error of a strongly nonlinear problem still has a useful linear expression, at least as far as our analysis of the error has progressed.

In contrast to the fourth approach to uncertainty quantification above, we allow for errors generated within the solution pROcesses. Thus we subsume and expand on this point of view.

As a technical introduction to the paper, we study errors of a spherical shock interaction problem on uniform radial grid of 100 and 500 cells (with errors determined by reference to a 2000 cell calculation referred to as the fine grid). We use MUSCL [1] as the numerical method; for the comparison of tracked to untracked solutions of the problem, see [3]. The equation of state is a γ-law gas with $\gamma = 5/3$. The ensemble of 200 initial conditions is defined by a Latin hypercube variation shock and contact strength by $\pm 10\%$ about a base case defined (as in [4]) by a contact located at 1.5 units from the origin; an inward moving shock located 2.25 units from the origin, with all constant states between waves. The initial base case shock strength is $M = 32.7$ and the initial base case Atwood number for contact is 0.82.

2. The Statistical Numerical Riemann Problem

We study statistical numerical Riemann problems (SNRP) in spherical geometry. The SNRP introduces errors (modeled as random) in addition to propagating errors or uncertainty from input to output. The waves in the SNRP have a finite width and the solution algorithm in the SNRP has only finite accuracy. Because of the possible finite width of the input waves, the problem and its solution are not strictly scale invariant. Moreover scale invariance is lost through the length scale introduced by the radius at the time of interaction.

We consider a generalization of the spherically symmetric Riemann problem. A statistical distribution of numerical incoming waves and starting states determines the SNRP. Its solution gives the output waves, each of which generate the same type of data. Thus we define the SNRP as a statistical (non-deterministic) mapping from a statistical input wave description to a statistical output wave description.

The statistics of the SNRP mapping function arise from grid errors, and from the random placement of a traveling wave relative to the centers of the finite difference lattice. Our objective in this section is to build up a library of statistical input-output relations that will include all Riemann problems to be encountered in Sec. 3. This library will be used to predict results for the composite, late time, or multi-wave error and uncertainty analysis based on a multi-path scattering formula, as developed in [4]. The input to the multi-path scattering error prediction formula is elementary, in that it consists of errors associated with individual isolated wave interactions and input error uncertainty only.

2.1. The Single Propagating Wave. We start with the analysis of the single propagating inward shock in spherical geometry. The radially dependent strength of convergent spherical shocks is discussed in [8]. The spatial variation of convergent spherical shocks is contained in the Guderley solution [7]. The inward moving shocks are not of constant strength as in a planar geometry, but evolve approximately according to a power law as a function of the radius. From Whitham's approximation approach, we have

$$M \propto r^{-1/n}, \tag{2.1}$$

for cylindrical shocks, and

$$M \propto r^{-2/n}, \tag{2.2}$$

for spherical shocks. Here M is the Mach number of the shock, $n = 1 + \frac{2}{\gamma} + \sqrt{\frac{2\gamma}{\gamma-1}}$, and γ is the adiabatic exponent defined as the ratio of two specific heats. A comparison with the exponents from Guderley's exact similarity solution is given in Table 2.1. We also have a similar approximate power law for the shock velocity.

TABLE 1. Comparison of the exponents from the approximate and the exact similarity solutions for an inward propagating spherical shock wave.

	Cylindrical		Spherical	
γ	Approximate	Exact	Approximate	Exact
6/5	0.163112	0.161220	0.326223	0.320752
7/5	0.197070	0.197294	0.394142	0.394364
5/3	0.225425	0.226054	0.450850	0.452692

Fig. 1 shows the exponential divergence of the shock strength (here characterized by the Mach number) at $r \to 0$. The accuracy is amazing in view of the simplicity of the approximate theory. The figure shows that converging shocks are reacting primarily with the geometry, as assumed in the approximate theory, and

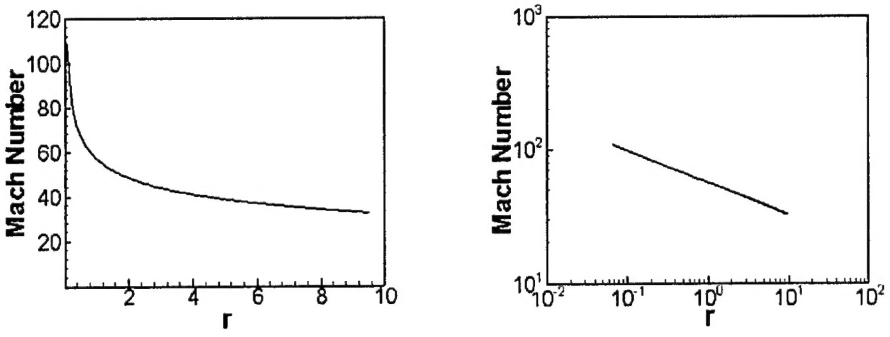

FIGURE 1. Left. Mach number *vs.* radius for a single inward propagating shock. Right. The same data plotted on a log-log scale.

are affected very little by further disturbances from the source of the motion; the strength of the initial shock enters only through the constants of proportionality in (2.1) and (2.2). This is not true for outward moving shocks. They slow down due to both the expanding geometry and to the continuing interaction with the flow behind. From Fig. 2, however, we find that the strength of an outward moving shock also follows a power law which is similar to (2.2) but with a modified exponent, after the radius of the outward moving shock is three times the initial radius. To develop a model for shock wave propagation which has a smaller pre-asymptotic regime, we allow two distinct exponents,

$$M \propto \begin{cases} r^{a_1} & r_0 \le r \le 3r_0 \\ r^{a_2} & r \ge 3r_0. \end{cases} \tag{2.3}$$

Here we choose $a_1 = -0.4$, $a_2 = -1.0$ for $\gamma = 1.67$, and r_0 is the initial shock radius.

We also study the single propagating contact (step up and step down cases). Fig. 3 shows the contact width $w_c \sim c_c t^{1/5}$ growing from 2 to 5 cells with a rate asymptotically proportional to $t^{1/5}$. We found that the step up contact and the step down contact have the same behavior. These properties appear to be sensitve to the details of the numerical algorithm. We have used a MUSCL algorithm. The degree of recalibration of the model as presented here, needed for other solvers, is an important question, out of the scope of the study. For some aspects of the solution error, the probabilistic error formalism is more general than is required. When the standard deviation of the error is much smaller than the mean error (when the coefficient of variation, their ratio, is close to zero), then the error is essentially deterministic, and the probabilistic formulation is unnecessary. This is the case in Fig. 3, with the standard deviation of the width, shown to the left scale of Fig. 3, significantly smaller than the mean width.

2.2. The Shock Contact Interaction. We study the wave strength, speed, width and position errors after a wave interaction. We represent the wave properties

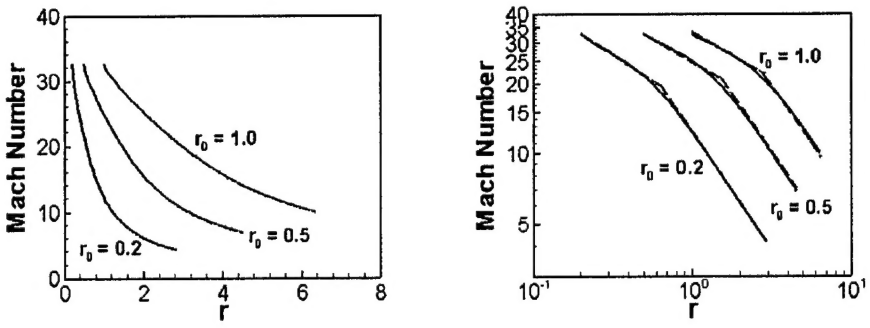

FIGURE 2. Left. Mach number *vs.* radius for an outward moving shock wave starting at different radii r_0. Right. The same data plotted on a log-log scale; the dashed lines in this plot represent the power law model (2.3).

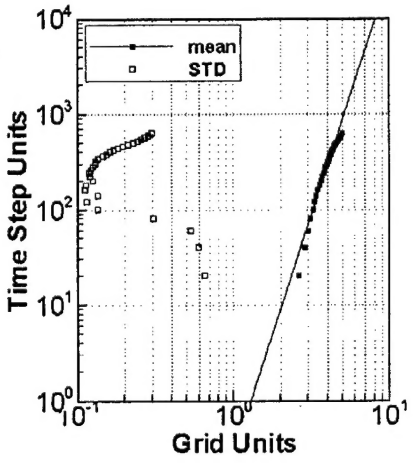

FIGURE 3. Ensemble mean contact width for a single propagating contact. We record the width in units of Δx. The standard deviation is also plotted, as the points to the extreme left.

as a five tuple

$$w_k^a = (\omega_k^a, \delta_k^a, \lambda_k^a, s_k^a, p_k^a) \ , \tag{2.4}$$

where ω is a wave strength, δ is an error in the wave strength, λ is a wave width, s is a wave speed error, and p is a position error. Also $a = i$ denotes input and $a = o$ signifies output. We choose dimensionless variables to measure wave strengths; the

Atwood number $A = (\rho_2 - \rho_1)/(\rho_2 + \rho_1)$ to measure the contact strength, and the Mach number M defined as the ratio of the shock speed to the ahead state sound speed, in the frame of a stationary ahead state, for the shocks. We measure the wave widths in units of mesh spacing. The wave position errors are specified in grid units, after an initial transient period. Within this formulation, we can describe the output wave errors by an expression multi-linear (and eventually linear) in the two input wave strengths, *i.e.* linear in each of the two input wave strengths.

For input wave strengths ω_1^i, ω_2^i (i denotes in) and output wave strengths ω_1^o, ω_2^o and ω_3^o (o denotes out) (ordered from left to right), the multinomial expansion for the output is defined by its coefficients $\alpha_{k,J}$, for J a multi index, $J = (j_1,\ j_2)$. The expansion has the form

$$\omega_k^o = \sum_J \alpha_{k,J} \omega^{i,J} \ , \tag{2.5}$$

where $\omega^{i,J} = (\omega_1^i)^{j_1}(\omega_2^i)^{j_2}$. The coefficients $\alpha_{k,J}$ depend parametrically on the base case Riemann problem, about which a specified variation is allowed. Given a statistical ensemble of input and output values ω^i and w^o, we use a least squares algorithm to determine the best fitting model parameters $\alpha_{k,J}$, for any given polynomial order of model. We use (2.5) variationally, that is to map input variation (about the base case for the ensemble) to output variability. In other words, (2.5), which is a formula for wave strengths, implies a similar formula with different but computable coefficients $\alpha_{k,J}$, in which all ω's are defined as variations from the base case, so that they represent uncertainty or error. In the planar case [4], we showed that a linear input-output relation, $\omega_k^o = \alpha_{k,0} + \sum_j \alpha_{k,j}\omega_j^i$ was sufficient to describe the exact (nonlinear) input-output relation. The adequacy of this model is established from consideration of the STD of the model error. We see that the same assumption is adequate in the present case. We also have an expansion similar to (2.5) for the wave strength errors, wave width errors and wave position errors. To avoid possible confusion, we note that the word error is used to describe two different types of quantities. The solution (wave strength, width or position) error is a difference between a fine grid and a coarse grid solution. The coefficients for a linear model of point values of this error are presented. The model error is the difference in some quantity and the linear model (2.5) to represent it, as a function of the variable parameters which define the ensemble.

We begin with the analysis of the initial shock contact SNRP at the ensemble averaged level. We present the linear model coefficients in Table 2, with $\pm 10\%$ variation for the initial contact strength and $\pm 5\%$ variation for the initial shock strength (consistent with $\pm 10\%$ variation in pressure ratio as used in the planar study [4]) about the base case. According to the analysis of Sec. 2.1, the strength of this initial inward shock is not constant, and is increasing as it moves toward the origin. We use the power law $M = Cr^{-2/n}$ to estimate the initial shock strength at the interaction time and use this quantity represented by the variable C as the input shock strength in the modeling. The input contact width has been set to zero, as part of the specification of this SNRP.

To read Table 2, we note that the first (ω_1^o) row (labeled in the table as ω_1^o (1. sonic)) lists coefficients $\alpha_{1,J}$ for $J = (0,0)$, $J = (1,0)$, *etc.* These coefficients are determined by a least squares algorithm that minimizes the expected, or mean error over the ensemble, in comparing the linear predictions to the exact solution of the Riemann problem. The last two columns describe errors in the model

TABLE 2. The SNRP shock contact interaction. Expansion coefficients for output wave strengths, wave strength errors, wave width errors and wave position errors (linear model) for the initial shock contact interaction. Here the base case input contact wave width is zero. The final columns refer to difference between the linear model (2.5) and the exact quantity. The errors in rows 4-12 refer to the difference between the numerical solution on 100 cells and the exact solution using 2000 cells.

variable \ coef	const	ω_1^i	ω_2^i	model error	
		(contact)	(l. sonic)	STD	STD/$\bar{\omega^o}$
wave strengths (100 cells)					
ω_1^o (l. sonic)	-33.353	19.521	2.501	0.860	0.954%
ω_2^o (contact)	0.374	0.200	0.0003	0.042	7.650%
ω_3^o (r. sonic)	3.568	0.402	-0.045	0.009	0.463%
wave strength errors (100 cells)					
δ_1^o (l. sonic)	2.039	-3.200	-0.01	0.157	0.174%
δ_2^o (contact)	0.236	0.016	-0.002	0.021	3.825%
δ_3^o (r. sonic)	0.053	0.003	-0.001	0.0008	0.041%
wave width errors (100 cells)					
λ_1^o (l. sonic)	1.675	0.305	0.017	0.085	
λ_2^o (contact)	7.093	0.482	-0.146	0.239	
λ_3^o (r. sonic)	2.829	0.302	-0.024	0.107	
wave position errors (100 cells)					
p_1^o (l. sonic)	-0.247	0.242	0.005	0.009	
p_2^o (contact)	0.643	0.065	-0.011	0.192	
p_3^o (r. sonic)	-0.042	0.062	0.004	0.009	

(2.5). The presence of outliers was monitored and the ensemble L_∞ norm determined (results not tabulated); occasional outliers indicate non Gaussian statistics. The model error is defined as (predicted - exact) where exact is the result of the simulation and predicted is the value given by the finite polynomial (linear) model (2.5). The column STD is the standard deviation of (predicted - exact). Note that the STD errors, as defined, are dimensionful. To aid in interpreting the error magnitudes, we present in a final column (labeled STD/$\bar{\omega^o}$) the standard deviation of the error in the model divided by the mean value of the variable predicted. This column represents a fractional (dimensionless) error in the model.

According to the analysis of Sec. 2.1, the strength of the output inward moving shock is modeled as $Cr^{-2/n}$. This formula is accurate after some time, and the

Table 2 entry is $\omega_1^o = C$ in this formula. We form a linear model for this constant in this expression in Table 2. We find very small errors in the exponent, not tabulated here. We developed a model (2.3) for the strength of the output outward moving shock in Sec. 2.1. Here in our study, we are only concerned with the first formula in (2.3). The entry ω_3^o in the table represents the coefficient multiplying the power term.

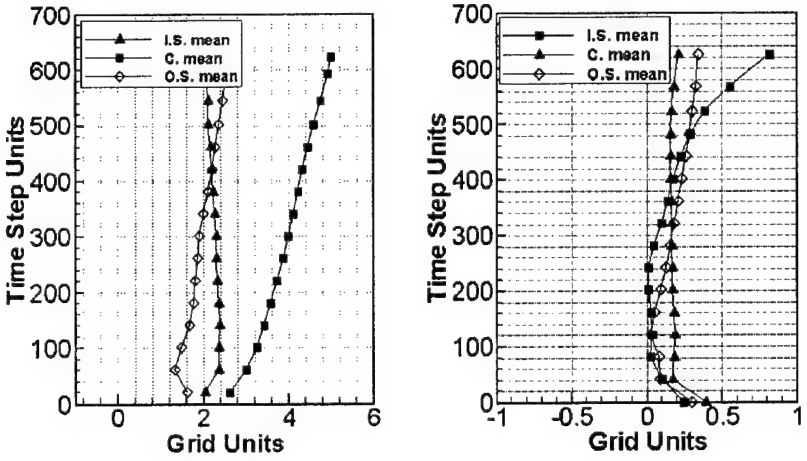

FIGURE 4. Left: ensemble mean inward/outward moving shock and contact widths after a shock contact interaction. Right: ensemble mean shock and contact position errors as a function of time, expressed in grid units. The associated standard deviations are extremely small, not shown in the plots. In the legend, C. denotes the contact while I.S. and O.S. are the inward and outward moving shocks.

The three variable (λ) rows in Table 2 represent wave width errors. The standard deviation for this quantity is about 10% of the mean value, indicating that the error model is (on the whole) satisfactory, and that the shock wave widths are not (mostly) fluctuating greatly. The inward moving shock width decreased about 10% relative to the wave width at the interaction time, while the outward moving shock width increased about 10%. See Fig. 4, left frame. The contact width is modeled as $c_c t^{1/5}$ where both the width and t are expressed in mesh units. The Table 2 entry $\lambda_2^o = c_c$ in this formula. We form a linear model for this constant in this expression in Table 2.

We also study the wave position errors. Fig. 4, right frame, shows the position errors as a function of time. The entries in the wave position rows of Table 2 present those errors, given in mesh units. All position errors are subgrid. The standard deviations are smaller than the means, indicating that the errors are basically deterministic.

All solution errors are sensitive to the grid spacing, taken to be 100 computational cells in Table 2-4. This sensitivity is not extreme. For example, if the 100 cell

model is used to analyze the 500 cell data, the model errors (STD) approximately double, but remain small.

2.3. Shock Reflection at the Origin. Here we study the reflection of the shock off the origin. According to the analysis of Sec. 2.1, the input inward moving shock has infinite strength at the origin. We used the strength at the radius $r = 1$ as the initial state and the input shock strength in the modeling process. We study the wave strength, wave strength errors, wave width and wave position errors. See Table 3.

TABLE 3. The SNRP defined by the shock reflection at the origin. Expansion coefficients for output wave strengths, wave strength errors, wave width errors and wave position errors (linear model) for input variation ±10%.

variable \ coef	const	ω_1^i	model error	
		(l. sonic)	STD	STD/$\bar{\omega}^o$
ω_1^o (r. sonic)	-242.394	5.606	1.137	0.468%
δ_1^o (r. sonic)	-3.27	0.031	0.112	0.045%
λ_1^o (r. sonic)	1.221	0.018	0.099	
p_1^o (r. sonic)	0.474	0.001	0.012	

We found that the Mach number of the outward moving shock (reflected shock) was essentially independent of the input variation in Mach number. To explain this phenomena, we recall that the ambient state ahead of the outward moving reflected shock is an incoming continuously variable flow. The sound speed ahead of this flow is affine linearly dependent on the strength of the incoming shock wave, as is the shock speed of the reflected outward moving shock wave. Thus the outward moving Mach number, as a ratio of two quantities varying affine linearly with the incoming shock strength, has a fractional linear form in the incoming wave strength. A simple calculation shows that the variation in the outward moving shock Mach number M_o contains the factor $(1 - M_o)$ and since $M_o \approx 1.2$, this small factor suppressed variation in M_o as a function of M_i, the Mach number of the incoming shock. Thus the Mach number is not a good measure for the outward moving shock strength. We choose the pressure behind the reflected shock instead as ω_1^o in Table 3. The pressure also follows the power law. The large entries in this row result from the fact that the (dimensional) pressure (ω_1^o) is much larger in pressure units than the Mach number (ω_1^i).

2.4. The Contact Reshock Interaction. After reflection from the origin, the transmitted lead shock wave re-crosses the deflected contact. The outgoing waves from this interaction consist of a rarefaction wave propagating toward the origin, a contact and a shock propagating outward. The region inside of the outward propagating shock, on both sides of the contact is not piecewise constant, but contains an inward propagating compression, which eventually breaks to form an inward moving shock, reaching the origin at interaction 4. This inward moving

TABLE 4. The SNRP contact reshock interaction. Expansion coefficients for output wave strengths, wave strength errors, wave width errors and wave position errors (linear model).

variable \ coef	const	ω_1^i (r. sonic)	ω_2^i (contact)	model error STD	model error STD/$\bar{\omega^o}$
wave strengths (100 cells)					
ω_1^o (l. sonic)	0.097	-0.108	0.436	0.031	13.305%
ω_2^o (contact)	0.103	-0.192	1.168	0.007	1.116%
ω_3^o (r. sonic)	0.988	0.195	-0.225	0.003	0.262%
wave strength errors (100 cells)					
δ_1^o (l. sonic)	-0.291	0.161	-0.468	0.017	7.296%
δ_2^o (contact)	-0.067	0.142	-0.125	0.006	0.957%
δ_3^o (r. sonic)	-0.030	0.107	-0.0004	0.001	0.087%
wave width errors (100 cells)					
λ_1^o (l. sonic)	9.776	-6.372	5.091	0.484	
λ_2^o (contact)	1.903	0.156	-0.677	0.534	
λ_3^o (r. sonic)	4.088	-1.401	1.549	0.168	
wave position errors (100 cells)					
p_1^o (l. sonic)	4.782	-3.602	2.372	0.379	
p_2^o (contact)	-0.453	0.409	-0.054	0.177	
p_3^o (r. sonic)	-0.199	-0.685	3.213	0.052	

compression is generated from the geometrically caused weakening of the outward moving shock, and is a well recognized aspect of spherical shock wave dynamics. The shock and the rarefaction interact, and eventually the rarefaction disappears in this interaction. Here we only follow the waves through the output of interaction 3, and thus avoid much of this interaction. Specifically, we focus on the inward moving rarefaction and not the inward moving shock. We study the wave strength, wave strength errors, wave width and wave position errors resulting from interaction 3. See Table 4.

According to the analysis of Sec. 2.1, this is a step down interaction and the contact width is modeled as $c_c t^{1/5}$ where both the width and t are expressed in mesh units. We form a linear model for the coefficient c_c in this expression in Table 4. The rarefaction width has the form constant + rate $\times$ time. The entry λ_1^o refers to the constant, which gives an offset for the centering of the rarefaction wave. This entry is expressed in mesh units.

3. Composite Shock Interaction Problems

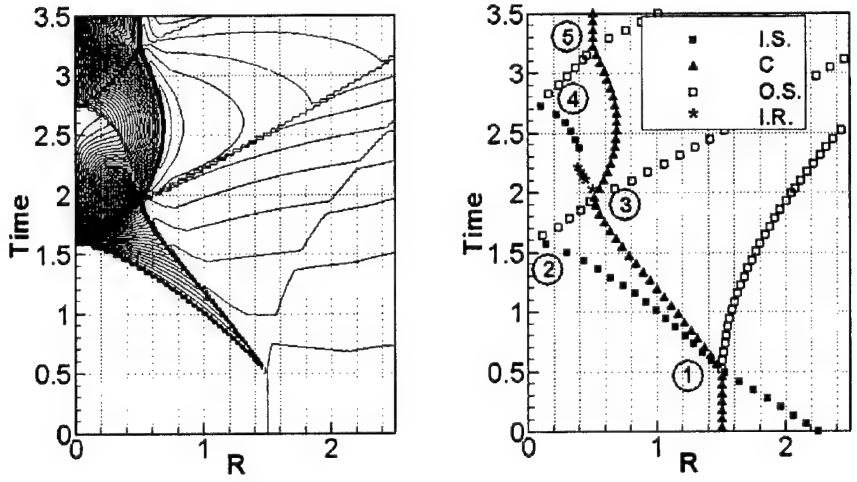

FIGURE 5. Left: space time density contour plot for the multiple wave interaction problem studied in this section, in spherical geometry. Right: type and location of waves determined by the wave filter analysis with labels for the interactions. Here I.R. denotes the inward moving rarefaction.

We consider the repeated interactions of a spherically symmetric shock wave with a spherical contact located near the origin. The base case for each wave interaction coincides with the base case assumed for the interactions studied in Sec. 2. The transmitted shock, after interaction with the contact, progresses to interact with (*i.e.* reflect off) the origin. This interaction was also studied in Sec. 2. Subsequently, there are a number of reverberations, of reflected rarefactions and compression waves, between the contact and the origin. The interactions are illustrated by the space time contour plots of the density, shown in Fig. 5, left. In Fig. 5 (right), we show the type and location of the waves, as determined by the wave filter analysis program. Five interactions are extracted from the complex wave interaction problem. Both figures refer to the base case. The build up of complex wave patterns is evident.

The main point of this section is to formulate and validate the multipath scattering formula of [4] for analysis of errors. We analyze errors at the output to interaction 3 directly, comparing the 100 mesh and 500 mesh simulation to a 2000 mesh, fine grid simulation, here taken as a substitute for the exact solution. These errors are compared to those generated by adding up and propagating errors from the input data and from each of the interactions 1 to 3, using the multipath scattering formula. Thus, for example, a position error as input to interaction 1 is translated geometrically to a position error for the output to interaction 1 via simple geometric considerations as in [4]. This error is propagated to an input error for

TABLE 5. Predicted and simulated errors for output wave strengths, wave widths and wave positions, output to interaction 3. The inward rarefaction and contact strengths are expressed dimensionlessly as Atwood numbers. The outward shock strengths are in the units of Mach number. The width and position errors are in mesh units. The wave strength errors are expressed as mean $\pm$ 2σ where σ is the ensemble STD of the error/uncertainty.

variable \ error	Simulation	Prediction	Simulation	Prediction
	100 *vs.* 2000 mesh		500 *vs.* 2000 mesh	
	wave strength errors and propagated initial uncertainties			
δ_1^o (l. sonic)	0.04±2(0.03)	0.03±2(0.02)	0.01±2(0.02)	0.009±2(0.01)
δ_2^o (contact)	0.14±2(0.05)	0.12±2(0.02)	0.03±2(0.01)	0.03±2(0.008)
δ_3^o (r. sonic)	-0.02±2(0.02)	-0.02±2(0.01)	-0.006±2(0.005)	-0.007±2(0.004)
	mean wave width errors		mean wave width errors	
λ_1^o (l. sonic)	3.04	2.83	2.63	2.72
λ_2^o (contact)	5.36	6.11	5.56	6.08
λ_3^o (r. sonic)	2.71	3.04	2.92	2.98
	mean wave position errors		mean wave position errors	
p_1^o (l. sonic)	1.25	0.23	0.12	0.18
p_2^o (contact)	0.43	0.06	0.05	0.04
p_3^o (r. sonic)	-0.73	-0.15	-0.08	-0.11

interaction 2 through solutions of radial differential equations. Propagation continues, and yields an error at the output to interaction 3. See Table 5. The wave strength rows present the result of initial uncertainty propagated to the output of interaction 3 as well as the accumulation of solution errors. The multipath scattering formula gives reasonable prediction of error magnitudes in all cases except the wave position errors for the under resolved (100 mesh) simulation. We see that the created numerical solution errors are important. We also find that a major portion of the created numerical solution errors come from the second interaction, the shock reflection interaction. A detailed study of these errors and their relative importance will be presented in a following paper.

4. High Dimensional Wave Filter

4.1. The Two Pass Algorithm. We develop a two dimensional wave filter. The analysis starts at a general point, and at that point, searches in a general direction. The analysis proceeds in two passes. The first pass uses only state data along a line segment, which are extracted from the 2D simulation data and analyzed using the 1D filter introduced previously [4]. In this first pass, we choose the normal direction as the direction through the given point which has the strongest wave in the dominant family and the weakest waves in the other families. We obtain an approximate wave position and width by applying the 1D filter to the line segment in the normal direction of the wave. The second pass improves in this choice of

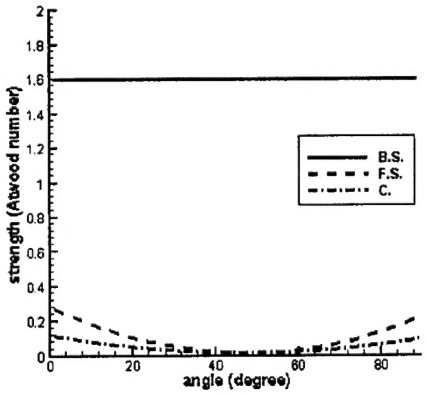

FIGURE 6. The strengths of 3 output waves.

normal direction by the construction of a local tangent plane. We introduce an array of (two in 2D) additional 1D line segments displaced tangentially (*i.e.* normal to the normal just constructed) from the original one. The analysis as above along each segment in the array leads to wave positions in the tangentially displaced array. Finally a tangent plane is fit to array of wave positions. The normal to this plane is the wave normal of the final construction. We analyze the inward moving shock wave before interaction 1 of our base case using this wave filter.

4.2. Initial Estimate for the Normal Direction of the Wave. Applying a 1D wave filter to the state data along a line segment gives a wave position and the width. Starting from a trial wave position, and a trial normal direction given by an angle θ, and a distance r along the resulting segment, we pick up two points on the left and the right ends of the segment. With the suitable choice of r, (e.g. the wave width) the states at the two points represent the left and right constant states of the wave. The left and right states and their decomposition into 1D elementary wave via a Riemann solution varies according to θ. The Riemann solution has three output waves, whose strengths are assessed dimensionlessly. The type of the strongest wave is defined to be the wave type at the trial wave position. The strongest wave has a maximum value and the weaker waves have minimum value at an angle θ_m. We choose θ_m as the normal direction. Using this normal direction θ_m, the 1D wave filter will select a trial position p_m and a wave width. Fig. 6 shows the strengths of three output waves at an angle $\theta, 0 \leq \theta \leq 90°$.

4.3. Corrected Estimate for the Normal Direction of the Wave. The accuracy of the wave position and normal is improved through the construction of a local patch of a wave surface. The 2D wave surface patch is a curve segment defined by two linear segments meeting at P_m, and thus defined (in the present approximation) by two points P_l and P_r, serving as end points of the two linear segments. We construct trial points P_l', P_r' by their locations along the tangential directions $\theta_m - 90°, \theta_m + 90°$ respectively passing through P_m at a certain distance d. Two normal direction θ_l, θ_r at P_l', P_r' respectively are found as above. Using

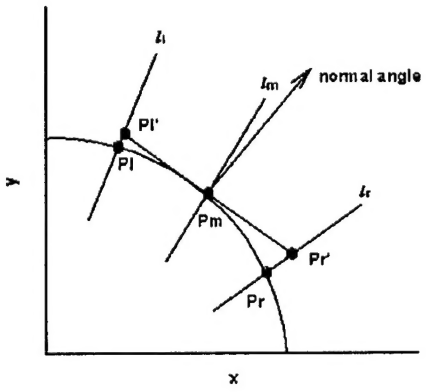

FIGURE 7. Schematic diagram illustrating the computation of the corrected estimate for the normal to the wave.

the 1D (first pass) construction along the lines defined by θ_l, P_l' and θ_r, P_r', we find two points P_l, P_r on the interface to define the local wave surface patch. With these three points, P_l, P_m, P_r on the interface, we can construct a circle. This circle represents the interface locally. The normal direction θ_n of the circle at the point P_m represents the normal direction of the interface at the point P_m. We choose θ_n as the normal direction for the correction step.

Fig. 7 shows a schematic diagram illustrating the correction step. We see the correction from the initial estimate l_m to the corrected normal.

The correction depends on the distance d from P_m to P_l' and P_r'. If d is too small, the normal direction is sensitive to the error in the points P_l, P_r on the interface. Fig. 8 shows that the choice of d equal to 3 mesh units is satisfactory. This figure also illustrates the improvement of accuracy and the robustness of the correction step. Here, we tested 89 lines at angles $1 - 89°$ for θ_0 from $(0,0)$ for P_0 to the initial shock data, input to interaction 1 of our base case simulation. We see that the standard deviations of the errors for the normal direction are small. The space averages of the errors for the normal direction, which we do not present, were very small (less than 10% of the STD) for all choices of d. All choices of d give a satisfactory normal direction. The initial errors are somewhat large. This is because the wave has 0 wave width at the initial time step. The 1D filter fits state data to an error function, and this fit is not stable before the initialization transients in the numerical shock have disappeared.

5. Conclusion

The multipath integral formula to express solution error as a composition of errors associated with individual interactions and a propagation law for errors between interactions has been extended to spherically symmetric shock interaction problems. The main new difficulties encountered were the non-constancy of the solution between interaction events and the non-constancy of waves and errors between interactions. In addition, as preparation for future multidimensional error

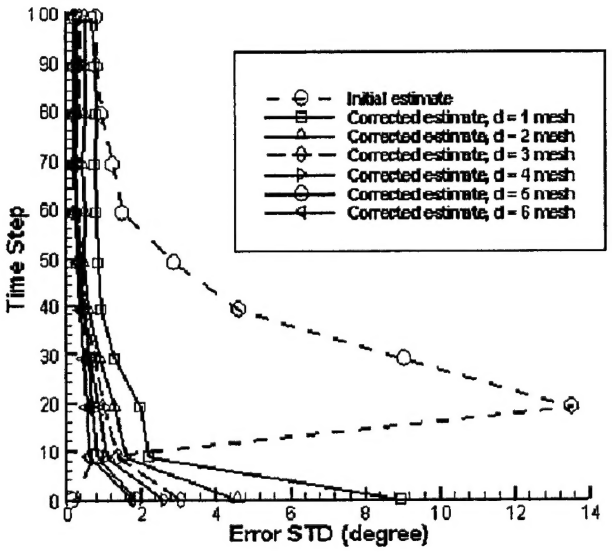

FIGURE 8. STD of errors for the wave normal constructed from the 2D wave filter, as a function of the tangential separation d of the wave front points P'_l, P'_r, in mesh units.

analysis, we have extended the wave filter previously introduced to detect waves in multidimensional numerical solutions.

References

[1] P. COLELLA, *A direct Eulerian MUSCL scheme for gas dynamics*, SIAM J. Comput., 6 (1985), pp. 104–117.

[2] B. DEVOLDER, J. GLIMM, J. W. GROVE, Y. KANG, Y. LEE, K. PAO, D. H. SHARP, AND K. YE, *Uncertainty quantification for multiscale simulations*, Journal of Fluids Engineering, 124 (2002), pp. 29–41. LANL report No. LA-UR-01-4022.

[3] S. DUTTA, J. GLIMM, J. W. GROVE, D. H. SHARP, AND Y. ZHANG, *Error comparison in tracked and untracked spherical simulations*, Computers and Mathematics with Applications, (2003). accepted, University at Stony Brook preprint number AMS-03-10 and LANL report No. LA-UR-03-2920.

[4] J. GLIMM, J. W. GROVE, Y. KANG, T. LEE, X. LI, D. H. SHARP, Y. YU, K. YE, AND M. ZHAO, *Statistical riemann problems and a composition law for errors in numerical solutions of shock physics problems*, SISC, (2003). (submitted) University at Stony Brook Preprint Number SB-AMS-03-11, Los Alamos National Laboratory number LA-UR-03-2921.

[5] J. GLIMM AND D. H. SHARP, *Stochastic methods for the prediction of complex multiscale phenomena*, Quarterly J. Appl. Math., 56 (1998), pp. 741–765.

[6] ——, *Prediction and the quantification of uncertainty*, Physica D, 133 (1999), pp. 152–170.

[7] G. GUDERLEY, *Starke kugelige und zylindrische verdichtungsstösse in der Nähe des kugelmittelpuktes bzw der zylinderachse*, Luftfahrtforschung, 19 (1942), pp. 302–312.

[8] G. B. WHITHAM, *Linear and Nonlinear Waves*, John Wiley & Sons, New York, 1974.

Department of Applied Mathematics and Statistics, State University of New York at Stony Brook, Stony Brook NY 11794-3600, or, Center for Data Intensive Computing, Brookhaven National Laboratory, Upton NY 11973

Los Alamos National Laboratory, Los Alamos, NM 87545
E-mail address: jgrove@lanl.gov

Los Alamos National Laboratory, Los Alamos, NM 87545
E-mail address: ykang@lanl.gov

Department of Applied Mathematics and Statistics, State University of New York at Stony Brook, Stony Brook NY 11794-3600
E-mail address: twlee@ams.sunysb.edu

Department of Applied Mathematics and Statistics, State University of New York at Stony Brook, Stony Brook NY 11794-3600
E-mail address: linli@ams.sunysb.edu

Los Alamos National Laboratory, Los Alamos, NM 87545
E-mail address: dhs@t13.lanl.gov

Department of Applied Mathematics and Statistics, State University of New York at Stony Brook, Stony Brook NY 11794-3600
E-mail address: kye@ams.sunysb.edu

Department of Applied Mathematics and Statistics, State University of New York at Stony Brook, Stony Brook NY 11794-3600
E-mail address: yan2000@ams.sunysb.edu

Department of Applied Mathematics and Statistics, State University of New York at Stony Brook, Stony Brook NY 11794-3600
E-mail address: mingzhao@ams.sunysb.edu